Nonlinear Entropy Transfer in ETG-TEM Turbulence via TEM Driven Zonal Flows

Yuuichi ASAHI, Akihiro ISHIZAWA[1)], Tomohiko WATANABE[2)], Hideo SUGAMA[1)], Hiroaki TSUTSUI and Shunji TSUJI-IIO

Tokyo Institute of Technology, Tokyo 152-8550, Japan
[1)]*National Institute for Fusion Science, Gifu 509-5292, Japan*
[2)]*Department of Physics, Nagoya University, Nagoya 464-8602, Japan*

(Received 4 November 2014 / Accepted 5 March 2015)

Nonlinear interplay of the electron temperature gradient (ETG) modes and the trapped electron modes (TEMs) was investigated by means of gyrokientic simulation. Focusing on the situation where both TEMs and ETG modes are linearly unstable, the effects of TEM-driven zonal flows on ETG turbulence were examined by means of entropy transfer analysis. In a statistically steady turbulence where the TEM driven zonal flows are dominant, it turned out that the zonal flows meditate the entropy transfer of the ETG modes from the low to high radial wavenumber regions. The successive entropy transfer broadens the potential fluctuation spectrum in the radial wavenumber direction. In contrast, in the situation where ETG modes are unstable but TEMs are stable, the pure ETG turbulence does not produce strong zonal flows, leading to a rather narrow spectrum in the radial wavenumber space and a higher transport level.

Keywords: gyrokinetic, turbulence, transport

DOI: 10.1585/pfr.10.1403047

1. Introduction

Microinstabilities in toroidal plasmas have received much attention due to their potential contribution to anomalous heat and particle transport. In a low-beta operation, it is often believed that the anomalous transport stems from drift wave turbulence driven by microinstabilities such as ion temperature gradient (ITG) mode [1], trapped electron mode (TEM) [2] and electron temperature gradient (ETG) mode [3,4]. The drift wave turbulence described by the gyrokinetic theory has been extensively investigated by numerical simulations (see the review paper [5]). As for the ion heat transport, the first principle gyrokinetic simulations of the ITG turbulence yield physically reasonable results and are used to construct a simplified transport model [6, 7].

It is widely accepted that reduction of turbulent fluctuations is brought by an $\mathbf{E} \times \mathbf{B}$ flow shear, especially, by the zonal flow shear [8]. This idea works well for the ITG turbulence. Still difficult to answer is whether the zonal flow plays a leading role in the ETG turbulence. There are two reasons for this: (i) the zonal flows produced by ETG modes are much weaker than those driven by ITG modes [3, 4] and (ii) the $\mathbf{E} \times \mathbf{B}$ shearing rate of the ITG-driven zonal flows is often much lower than a typical growth rate of the ETG modes [9]. So far, less attention has been paid to the TEM-driven zonal flows, while they may have a relatively smaller spatial scale than ITG-driven zonal flows. As the zonal flows with shorter wavelengths would have larger shearing rates, the TEM-driven zonal flow may be effective for the reduction of ETG fluctuations.

In our previous work, we investigated the influence of TEM-driven zonal flows on ETG turbulence and showed that the ETG turbulence can be regulated by the meso-scale TEM-driven zonal flows [10]. It was also shown that the $\mathbf{E}\times\mathbf{B}$ shearing rate of the TEM-driven zonal flows is larger than or comparable to the growth rates of long-wavelength ETG modes and TEMs which are likely to contribute to the electron heat transport. In the present paper, for a better understanding of the regulation mechanism of ETG turbulence by the TEM-driven zonal flows, we examined the nonlinear interactions of the ETG modes and TEM driven zonal flows.

A promising way to analyze the nonlinear interactions between the zonal flows and turbulence is the nonlinear entropy transfer analysis [11–13] which evaluates the nonlinear interactions of three different modes in the wavenumber space. In Refs. [11, 12], the influence of ITG-driven zonal flows on ITG turbulence was investigated by means of the entropy transfer analysis. It has been shown that the fluctuation spectra are broadened into the high radial wavenumber region as a consequence of successive entropy transfer [11, 12]. In accordance with the entropy transfer analysis in ITG turbulence, we apply it to the ETG-TEM turbulence to study the influence of the TEM-driven zonal flows on ETG turbulence. We can directly evaluate

author's e-mail: y.asahi@nr.titech.ac.jp

how the different scales of instabilities, that is ETG modes and TEMs in this case, interact via zonal flows. The result is discussed in comparison with those for ITG turbulence.

This paper is organized as follows. In Sec. 2, we present the electrostatic gyrokinetic equations and the entropy balance relation used in this study. Nonlinear simulation results including the entropy balance relation and the dynamics of zonal flows are presented in Sec. 3. In Sec. 4, we discuss the role of the TEM-driven zonal flows in the ETG-TEM turbulence based on the findings by nonlinear entropy transfer analysis. The obtained results are summarized in Sec. 5.

2. Simulation Model

Since the subject of this work is the entropy transfer analysis on our previous simulation data, the simulation model employed in this work is completely the same as that in Ref. [10]. Thus, we omit the model explanation and simply write down the nonlinear electrostatic gyrokinetic equation and the Poisson equation (see the details in Refs. [10, 14, 15]). Rather, we describe in detail the entropy balance equations [11, 16] that are more relevant to this work.

2.1 Governing equations

In the wavenumber space, the electrostatic gyrokinetic equation and the Poisson equation for the perturbed gyrocenter distribution function $\delta f_{sk_\perp}$ are written as follows:

$$\left[\frac{\partial}{\partial t} + v_\parallel \mathbf{b}\cdot\nabla + i\omega_{\mathrm{D}s} - \frac{\mu}{m_s}\left(\mathbf{b}\cdot\nabla B\frac{\partial}{\partial v_\parallel}\right)\right]\delta f_{sk_\perp} - \frac{c}{B_0}\sum_{k_\perp=k_\perp'+k_\perp''}\mathbf{b}\cdot(\mathbf{k}_\perp'\times\mathbf{k}_\perp'')\,\delta\psi_{k_\perp'}\delta f_{sk_\perp''} = F_{\mathrm{M}s}\left(i\omega_{*s} - i\omega_{\mathrm{D}s} - v_\parallel\mathbf{b}\cdot\nabla\right)\frac{e_s\delta\psi_{k_\perp}}{T_s} + C_s, \quad (1)$$

and

$$k_\perp^2\lambda_{\mathrm{D_e}}^2 n_0\frac{\mathrm{e}\delta\phi_{k_\perp}}{T_\mathrm{e}} = \sum_s e_s\delta n_s^{(p)} = \sum_s e_s\left[\int d\mathbf{v}J_{0sk_\perp}\delta f_{sk_\perp} - n_0\frac{e_s\delta\phi_{k_\perp}}{T_s}\left(1-\Gamma_{0sk_\perp}\right)\right], \quad (2)$$

where $F_{\mathrm{M}s} = n_0\left(m_s/2\pi T_s\right)^{3/2}\exp[-(m_s v_\parallel^2 + 2\mu B)/2T_s]$ is the Maxwellian representing the equilibrium distribution function, and $\omega_{\mathrm{D}s}\,(\omega_{*s})$ means the magnetic (diamagnetic) drift frequency. The subscript s represents each plasma species, where $s = \mathrm{i}$ (e) is for ions (electrons). The background gradients of density and temperature are given by $L_n = |\nabla\ln n|^{-1}$ and $L_{T_s} = |\nabla\ln T_s|^{-1}$, respectively. $\delta\psi_{k_\perp}$ is the gyro-phase averaged electrostatic potential which is related to the potential evaluated at particle position $\delta\phi_{k_\perp}$ by $\delta\psi_{k_\perp} = J_{0sk_\perp}\delta\phi_{k_\perp}$. The collision operator is denoted by $C_s(\delta f_{sk_\perp})$ where we have employed the Lenard-Bernstein model collision operator. See Ref. [10] for more details.

As for the abbreviations in Eq. (2), $\lambda_{\mathrm{D_e}} = (T_\mathrm{e}/4\pi n_0\mathrm{e}^2)^{1/2}$ is the electron Debye length, $\delta n_s^{(p)}$ is the density evaluated at particle position, $J_{0sk_\perp} = J_0\left(k_\perp v_\perp/\Omega_s\right)$ and $\Gamma_{0sk_\perp} = I_0\left(b_s\right)\exp\left(-b_s\right)$ with the gyrofrequency Ω_s and $b_s = k_\perp^2\left(v_{\mathrm{t}s}/\Omega_s\right)^2$ where the zeroth-order Bessel function and the zeroth-order modified Bessel function are denoted by J_0 and I_0, respectively.

For the ETG turbulence study, instead of Eq. (2), the so-called adiabatic ion model is often employed where a characteristic wavelength of turbulence is assumed to be much shorter than the ion Larmor radius ρ_{ti} i.e. $k_\perp \gg \rho_{\mathrm{ti}}^{-1}$. Then, the ion density evaluated at particle position $\delta n_\mathrm{i}^{(p)}$ is approximated by

$$\delta n_\mathrm{i}^{(p)} = -n_0\frac{e_\mathrm{i}\delta\phi_{k_\perp}}{T_\mathrm{i}}, \quad (3)$$

with $J_{0\mathrm{i}k_\perp} \sim 0$ and $\Gamma_{0\mathrm{i}k_\perp} \sim 0$. This model can describe the ETG instability but not the TEM dynamics. In contrast, the kinetic ion model solving Eq. (1) for each species with Eq. (2) can deal with both the ETG modes and TEMs. We may find influences of TEMs on turbulence transport through a comparison of simulation results from these two models.

2.2 Entropy balance equation

For detailed analysis of nonlinear interactions, we introduce the entropy balance equation [11, 16] which is derived from Eqs. (1) and (2). By taking the velocity space integral and flux surface average of Eq. (1) multiplied by $\delta f_{sk_\perp}^*/F_{\mathrm{M}s}$ and taking the summation with its complex conjugate, we obtain the entropy balance equation for each wavenumber,

$$\frac{\partial}{\partial t}\left(\sum_s T_s\delta S_{sk_\perp} + W_{k_\perp}\right) = \sum_s\left(T_s\mathcal{F}_{sk_\perp} + T_s\mathcal{T}_{sk_\perp} + T_s\mathcal{D}_{sk_\perp}\right), \quad (4)$$

where

$$\delta S_{sk_\perp} = \left\langle\int d\mathbf{v}\frac{\left|\delta f_{sk_\perp}\right|^2}{2F_{\mathrm{M}s}}\right\rangle, \quad (5)$$

$$W_{k_\perp} = \frac{1}{4\pi}\left\langle\left[k_\perp^2 + \sum_s\frac{1}{\lambda_{\mathrm{D}s}^2}\left(1-\Gamma_{0s}\right)\right]\frac{\left|\delta\phi_{k_\perp}\right|^2}{2}\right\rangle, \quad (6)$$

$$\mathcal{F}_{sk_\perp} = \frac{q_{sk_\perp}}{T_s L_{Ts}} + \frac{\Gamma_{sk_\perp}}{L_{ps}}, \quad (7)$$

$$q_{sk_\perp} = Q_{sk_\perp} - \frac{5}{2}T_s\Gamma_{sk_\perp}, \quad (8)$$

$$Q_{sk_\perp} = \mathrm{Re}\left\langle\int d\mathbf{v}\frac{1}{2}(m_s v_\parallel^2 + 2\mu B)\delta f_{sk_\perp}\left(-i\frac{ck_y\delta\psi_{k_\perp}}{B_0}\right)^*\right\rangle, \quad (9)$$

$$\Gamma_{sk_\perp} = \mathrm{Re}\left\langle\int d\mathbf{v}\delta f_{sk_\perp}\left(-i\frac{ck_y\delta\psi_{k_\perp}}{B_0}\right)^*\right\rangle, \quad (10)$$

$$\mathcal{T}_{sk_\perp} = \sum_{p_\perp}\sum_{q_\perp} \mathcal{J}_s\left[\mathbf{k}_\perp|\mathbf{p}_\perp,\mathbf{q}_\perp\right], \tag{11}$$

$$\mathcal{D}_{sk_\perp} \equiv \left\langle \int d\mathbf{v} \frac{1}{F_{\mathrm{M}s}} \mathrm{Re}[C_s(\delta f_{sk_\perp}) h^*_{sk_\perp}] \right\rangle, \tag{12}$$

with the characteristic length of pressure gradient $L_{ps} = (L_n^{-1} + L_{Ts}^{-1})^{-1}$. The flux surface average is denoted by $\langle\rangle$ and the complex conjugate is shown by $*$ mark. The non-adiabatic part of the perturbed distribution function, $h_{sk_\perp}$, is defined by

$$h_{sk_\perp} = \delta f_{sk_\perp} + J_0\left(k_\perp \rho_{ts}\right) \frac{e_s \delta\phi_{k_\perp}}{T_s} F_{\mathrm{M}s}. \tag{13}$$

$\mathcal{J}_s\left[\mathbf{k}_\perp|\mathbf{p}_\perp,\mathbf{q}_\perp\right]$ in $\mathcal{T}_{sk_\perp}$ is called the triad entropy transfer function defined by

$$\mathcal{J}_s\left[\mathbf{k}_\perp|\mathbf{p}_\perp,\mathbf{q}_\perp\right] \equiv \delta_{k_\perp+p_\perp+q_\perp,0} \left\langle \frac{c}{B_0}\mathbf{b}\cdot(\mathbf{p}_\perp\times\mathbf{q}_\perp) \right.$$
$$\left. \int d\mathbf{v} \frac{1}{2F_{\mathrm{M}s}} \mathrm{Re}[\delta\psi_{p_\perp} h_{sq_\perp} h_{sk_\perp} - \delta\psi_{q_\perp} h_{sp_\perp} h_{sk_\perp}] \right\rangle, \tag{14}$$

where the wavanumber vectors $\mathbf{k}_\perp{}'$ and $\mathbf{k}_\perp{}''$ in Eq. (1) are replaced by $-\mathbf{p}_\perp$ and $-\mathbf{q}_\perp$, respectively, in order to emphasize the symmetry in the triad-interaction for three different modes. With this notation, the triad-interaction condition for three different modes can be written as $\mathbf{k}_\perp+\mathbf{p}_\perp+\mathbf{q}_\perp = 0$.

The triad entropy transfer function describes the entropy flow in the perpendicular wavenumber space. In Sec. 4, we investigate the interactions between turbulence and zonal flow via the analysis of triad entropy transfer function.

3. Simulation Results

In this section, we look back on the previous simulation results [10] in terms of entropy balance and zonal flow dynamics. The physical and numerical settings are found in Ref. [10]. Nonlinear simulations employing the adiabatic and kinetic ion models were performed to investigate the difference of the pure ETG turbulence and ETG-TEM turbulence [10]. The adiabatic ion model is used for the pure ETG turbulence, whereas the kinetic ion model is employed for the ETG-TEM turbulence. It was shown that the ETG and TEM turbulence are simultaneously regulated by the TEM-driven zonal flows in the ETG-TEM turbulence case. To understand the underlining physics for the regulation of the ETG turbulence by the TEM-driven zonal flow, we applied the entropy transfer analysis to the simulation data shown in Ref. [10] and clarified the role of the TEM-driven zonal flow.

3.1 Entropy balance relation

In this subsection, we investigate the time evolution of entropy variables (see Eqs. (5) - (12)) and discuss the differences in the simulation results from adiabatic and kinetic ion models. It should be remarked that the only difference in the above two simulations is the treatment of ions (see Eqs. (2) and (3)).

Figure 1 shows the time evolution of the entropy balance relation, where the summation of the time derivative terms $\frac{\partial}{\partial t}\left(\sum_s T_s \delta S_s + W\right)\left(= \sum_{k_\perp} \frac{\partial}{\partial t}\left(\sum_s T_s \delta S_{sk_\perp} + W_{k_\perp}\right)\right)$, the summation of the transport terms $\sum_s T_s \mathcal{F}_s\left(= \sum_s T_s \sum_{k_\perp} \mathcal{F}_{sk_\perp} = \sum_s \sum_{k_\perp} (q_{sk_\perp}/L_{Ts} + T_s\Gamma_{sk_\perp}/L_{ps})\right)$, and the dissipation terms $\sum_s T_s \mathcal{D}_s (= \sum_s T_s \sum_{k_\perp} \mathcal{D}_{sk_\perp})$ are plotted for the (a) adiabatic and (b) kinetic ion cases. The summation of entropy transfer term $\mathcal{T}_{sk_\perp}$ over $k_\perp$ is zero, that is $\sum_{k_\perp} \mathcal{T}_{sk_\perp} = 0$. Since $\Delta\left(= \frac{\partial}{\partial t}\left(\sum_s T_s \delta S_s + W\right) - \sum_s T_s \mathcal{F}_s - \sum_s T_s \mathcal{D}_s\right)$ is much smaller than the sum of the transport terms, the entropy balance relation is well satisfied for both simulations. Thus, these two simulations can be the subjects of the entropy transfer analysis [11] which are described in Sec. 4.

As shown in Figs. 1 (a) and (b), the initial increase

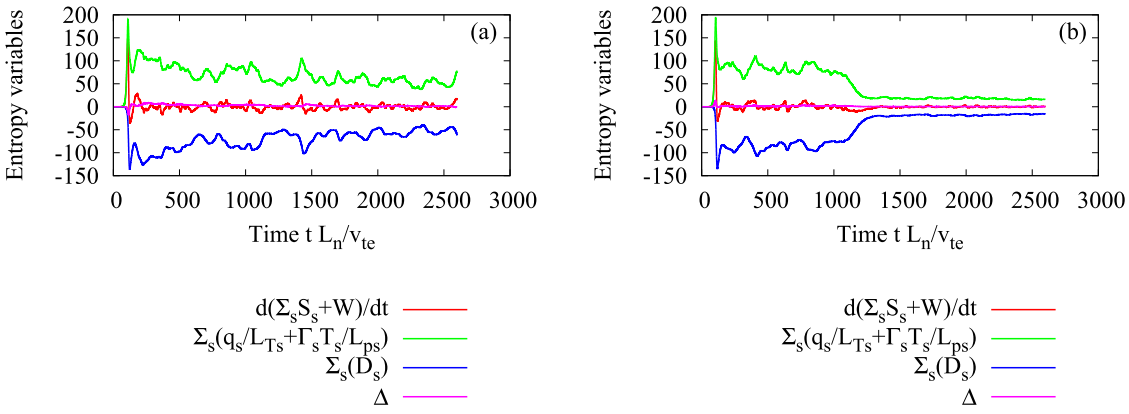

Fig. 1 The time evolution of the entropy variables defined in Eqs. (5) - (12) for (a) adiabatic ion (ai) model and (b) kinetic ion (ki) model. The numerical error Δ is much smaller than the summation of the transport terms, which means the entropy balance relation is satisfied in both simulations.

in the sum of the heat and particle transport due to the linear growth of ETG modes and a following statistical steady state are almost the same for the two cases until $t = 900\,(L_n/v_{te})$. The reduction of the transport at $t = 1200\,(L_n/v_{te})$ is found in the kinetic ion case, but not in the adiabatic ion case. After $t > 1400\,(L_n/v_{te})$, a statistically steady state is achieved in both cases, where the low transport level is sustained in the kinetic ion case. The difference in the transport level is explained by a difference in the zonal flow dynamics as described in Sec. 3.2.

3.2 Dynamics of zonal flow

To reveal the fundamental difference of zonal flows driven by ETG modes and by TEMs, we compare the squared amplitude of zonal flows calculated with the adiabatic and kinetic ion models. Although the ETG modes are unstable in both models, the TEMs are unstable only in the kinetic ion case. Figure 2 (a) shows the time evolution of the squared amplitude of zonal flows $\sum_{k_x}\langle|\delta\phi_{k_x,\,k_y=0}|^2\rangle$ calculated by the adiabatic and kinetic ion models. Here, k_x and k_y represent the radial and poloidal wavenumbers, respectively (Detailed definitions are found in Ref. [10]). While the ETG dominant phase before $t = 700\,(L_n/v_{te})$ is almost the same for the two cases, the zonal flow in the kinetic ion case grows again for $700\,(L_n/v_{te}) \le t \le 1200\,(L_n/v_{te})$ to achieve a larger amplitude in the statistical steady state than in the adiabatic ion case around $t \sim 2500\,(L_n/v_{te})$. The zonal flow structure is also compared in terms of the radial wavenumber spectra as shown in Fig. 2 (b). Both spectra have peaks at $k_x\rho_{te} = 0.044\,(k_x\rho_{ti} = 1.88)$, while the peak value is much higher in the kinetic ion case. According to the calculation of the residual zonal flow level for a wide wavenumber range covering both the ion and electron dynamics [17,18], zonal flows with $k_x\rho_{te} = 0.05\,(k_x\rho_{ti} = 2)$ are most likely to survive due to the less effective shielding effects of ions and electrons. The highest peak in the kinetic ion case is explained by the existence of the zonal flow drive, that is, the trapped electron mode whose characteristic wavenumber is about $k_y\rho_{ti} \sim 1$. Through the entropy transfer analysis in Sec. 4, it is shown that the zonal flow is driven in fact by the TEM in the kinetic ion case. Interactions between zonal flows and ETG turbulence are also investigated by means of the entropy transfer analysis.

4. Nonlinear Entropy Transfer Process

As shown in Sec. 3.2, the stronger zonal flow is generated in the kinetic ion case than in the adiabatic ion case. In order to identify the sources of zonal flows and to evaluate effects of zonal flows on ETG turbulence regulation, we investigated the nonlinear entropy transfer in the wavenumber space. Fluctuation spectrum of the ETG turbulence is also discussed in relation to the entropy transfer process.

4.1 Identification of zonal flow drive

Turbulent source of zonal flows (ZFs) are identified by the entropy transfer analysis in this subsection. Figure 3 shows the wavenumber spectra of the entropy transfer function $\overline{\mathcal{J}_e}\,[\mathbf{k_{ZF}}|\mathbf{p}_\perp, \mathbf{q}_\perp]$ for $k_{ZF}\rho_{te} = 0.044$ normalized to the sum of the transport terms $\overline{\mathcal{F}_{sk_\perp}}$ (defined in Eq. (7)). Hereinafter, the overlines on variables represent the time-average. The time-average is taken over $70\,(L_n/v_{te}) \le t \le 110\,(L_n/v_{te})$ $[1050\,(L_n/v_{te}) \le t \le 1150\,(L_n/v_{te})]$ for the transfer from ETG modes (TEMs) to zonal flow. The averaging period is estimated by the linear growth rate of ETG modes as $\tau_{ave} \sim \gamma_{ETG}^{-1} \sim 10\,(L_n/v_{te})$. Similarly, the averaging period for the TEM case is estimated by the linear growth rate of TEMs as $\tau_{ave} \sim \gamma_{TEM}^{-1} \sim 200\,(L_n/v_{te})$. The growth rates of ETG modes and TEMs are found in Fig. 1 in Ref. [10].

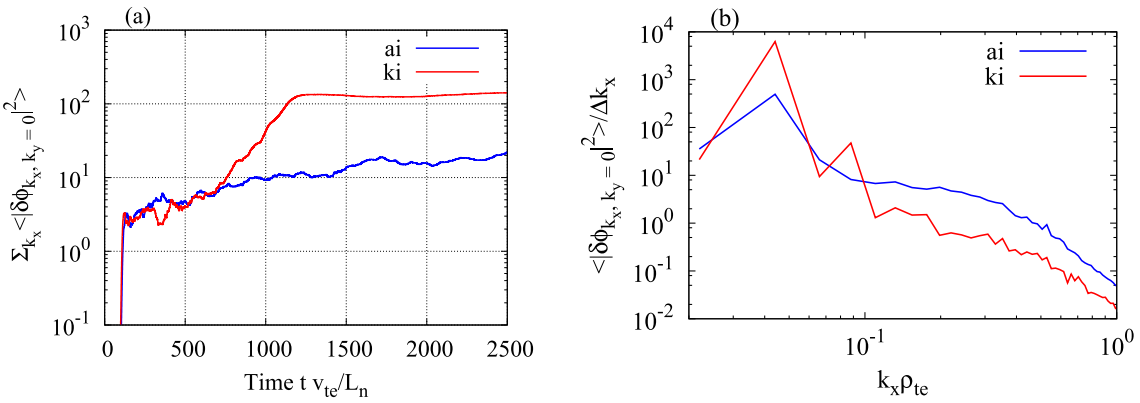

Fig. 2 Zonal component of electrostatic potential: (a) the time evolution of the squared amplitude of zonal flow potential $\sum_{k_x}\langle|\delta\phi_{k_x,\,k_y=0}|^2\rangle$, and (b) the time averaged wavenumber spectra of zonal flow $\langle|\delta\phi_{k_x,\,k_y=0}|^2\rangle/\Delta k_x$ calculated by adiabatic ion (ai) and kinetic ion (ki) simulation results, where the time-average is taken over $2300\,(L_n/v_{te}) \le t \le 2500\,(L_n/v_{te})$. The pure ETG turbulence and the ETG-TEM turbulence are found in the adiabatic and kinetic ion cases, respectively. The stronger zonal flow is driven in the kinetic ion case.

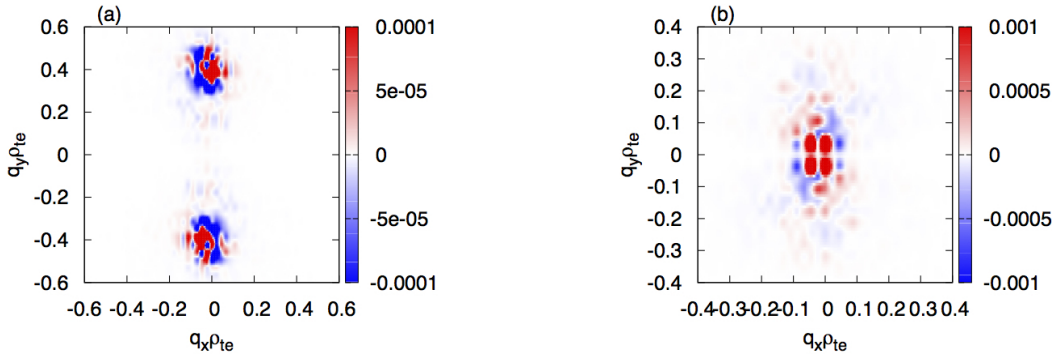

Fig. 3 Wavenumber spectra of the entropy transfer function normalized to the summation of the transport terms, $\overline{\mathcal{J}}_e\left[\mathbf{k_{ZF}}|\mathbf{p}_\perp,\mathbf{q}_\perp\right]/\overline{\mathcal{F}}_e$ for the zonal mode with $k_{ZF}\rho_{te} = 0.044$: (a) Zonal flow generation in the adiabatic ion case with the time-average for $70\,(L_n/v_{te}) \le t \le 110\,(L_n/v_{te})$ and (b) zonal flow generation in the kinetic ion case with time average for $1050\,(L_n/v_{te}) \le t \le 1150\,(L_n/v_{te})$. The zonal flow is initially driven by high wavenumber ETG modes both in the adiabatic and kinetic ion cases (a), and later driven by TEMs in the kinetic ion case (b).

As shown in Fig. 3 (a), peaks of $\overline{\mathcal{J}}_e\left[\mathbf{k_{ZF}}|\mathbf{p}_\perp,\mathbf{q}_\perp\right]/\overline{\mathcal{F}}_e$ in the adiabatic ion case are found at high wavenumber region around $q_y\rho_{te} \sim 0.4$. It means that the zonal flow is mainly driven by the high-wavenumber ETG modes. The spectrum of $\overline{\mathcal{J}}_e\left[\mathbf{k_{ZF}}|\mathbf{p}_\perp,\mathbf{q}_\perp\right]/\overline{\mathcal{F}}_e$ averaged over $70\,(L_n/v_{te}) \le t \le 110\,(L_n/v_{te})$ in the kinetic ion case (not shown) is almost the same as in the adiabatic ion case. This implies that the zonal flows are initially driven by the linearly unstable ETG modes.

In the later time for $t > 1050\,(L_n/v_{te})$ in the kinetic ion case, however, the zonal component receives the entropy from low wavenumber modes with $q_y\rho_{te} = \pm 0.035$ which correspond to the TEMs (see Fig. 3 (b)). The entropy transfer from the high wavenumber ETG modes is relatively small compared to the transfer from the low wavenumber TEMs. Our conclusion remains unchanged, even when we take the summation of the entropy transfer function for zonal flow, $\sum_{k_x}\overline{\mathcal{J}}_e\left[\mathbf{k_{ZF}}|\mathbf{p}_\perp,\mathbf{q}_\perp\right]/\overline{\mathcal{F}}_e$. As shown in Fig. 4, the zonal flow mainly receives the entropy from low wavenumber modes with $q_y\rho_{te} = \pm 0.035$, since the $(k_x, k_y) = (0.044, 0)$ mode is the dominant Fourier mode of zonal flows.

The above results manifest existence of the different sources of zonal flows, that is the ETG modes in the initial phase of the adiabatic and kinetic ion cases and the TEMs in the latter phase of the kinetic ion case.

4.2 Entropy transfer via zonal flow

In the steady state of ITG turbulence, it is reported that the zonal flow works as a mediator which transfers the entropy from the primary ITG modes to the higher radial-wavenumber modes [11]. By contrast, in the steady state of the pure ETG turbulence, zonal flows do not contribute to the successive entropy transfer in the radial wavenumber direction. In this context, the role of TEM driven zonal flows in the ETG-TEM turbulence was investigated. Figure 5 shows the wavenumber spectra of the entropy transfer

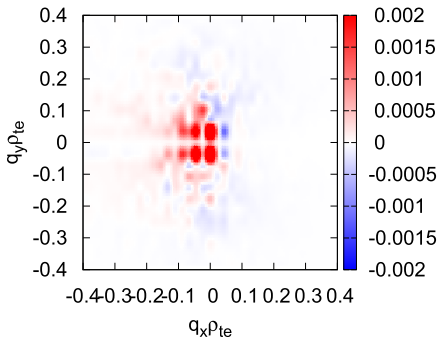

Fig. 4 Wavenumber spectra of the total entropy transfer from turbulence to zonal flow normalized to the summation of the transport terms, $\sum_{k_x}\overline{\mathcal{J}}_e\left[\mathbf{k_{ZF}}|\mathbf{p}_\perp,\mathbf{q}_\perp\right]/\overline{\mathcal{F}}_e$. The time average is taken over $1050\,(L_n/v_{te}) \le t \le 1150\,(L_n/v_{te})$. The zonal flow receives entropy mainly from TEMs with $q_y\rho_{te} = \pm 0.035$.

function $\overline{\mathcal{J}}_e\left[\mathbf{p}_\perp|\mathbf{q}_\perp,\mathbf{k}_\perp\right]/\overline{\mathcal{F}}_e$ for the adiabatic (Figs. 5 (a), (c) and (e)) and kinetic ion cases (Figs. 5 (b), (d) and (f)) with $\mathbf{p}_\perp \equiv (p_x\rho_{te},\ p_y\rho_{te}) = (0,\ 0.21)$, (0.044, 0.21) and (0.088, 0.21), respectively, where the ETG mode with $(p_x\rho_{te},\ p_y\rho_{te}) = (0,\ 0.21)$ has the largest amplitudes amid all the unstable modes. As is often the case, ETG turbulence shows the inverse-cascade process where the largest amplitude mode is shifted from the most unstable mode to lower wavenumber modes, since the energy is mainly transferred to larger scales (See for example, Ref. [19]). The change of dominant mode from $k_y\rho_{te} \sim 0.4$ to $k_y\rho_{te} \sim 0.2$ can also be considered as a typical inverse cascade process in ETG turbulence. The time average is taken over $2300\,(L_n/v_{te}) \le t \le 2500\,(L_n/v_{te})$, where the averaging period is estimated from the linear growth rate of TEMs as $\tau_{ave} \sim \gamma_{TEM}^{-1} \sim 200\,(L_n/v_{te})$.

In Fig. 5 (b), the two-stripe pattern at $p_y\rho_{te} = 0$ and $p_y\rho_{te} = -0.21$ is found which indicates that the $\mathbf{p}_\perp$ mode

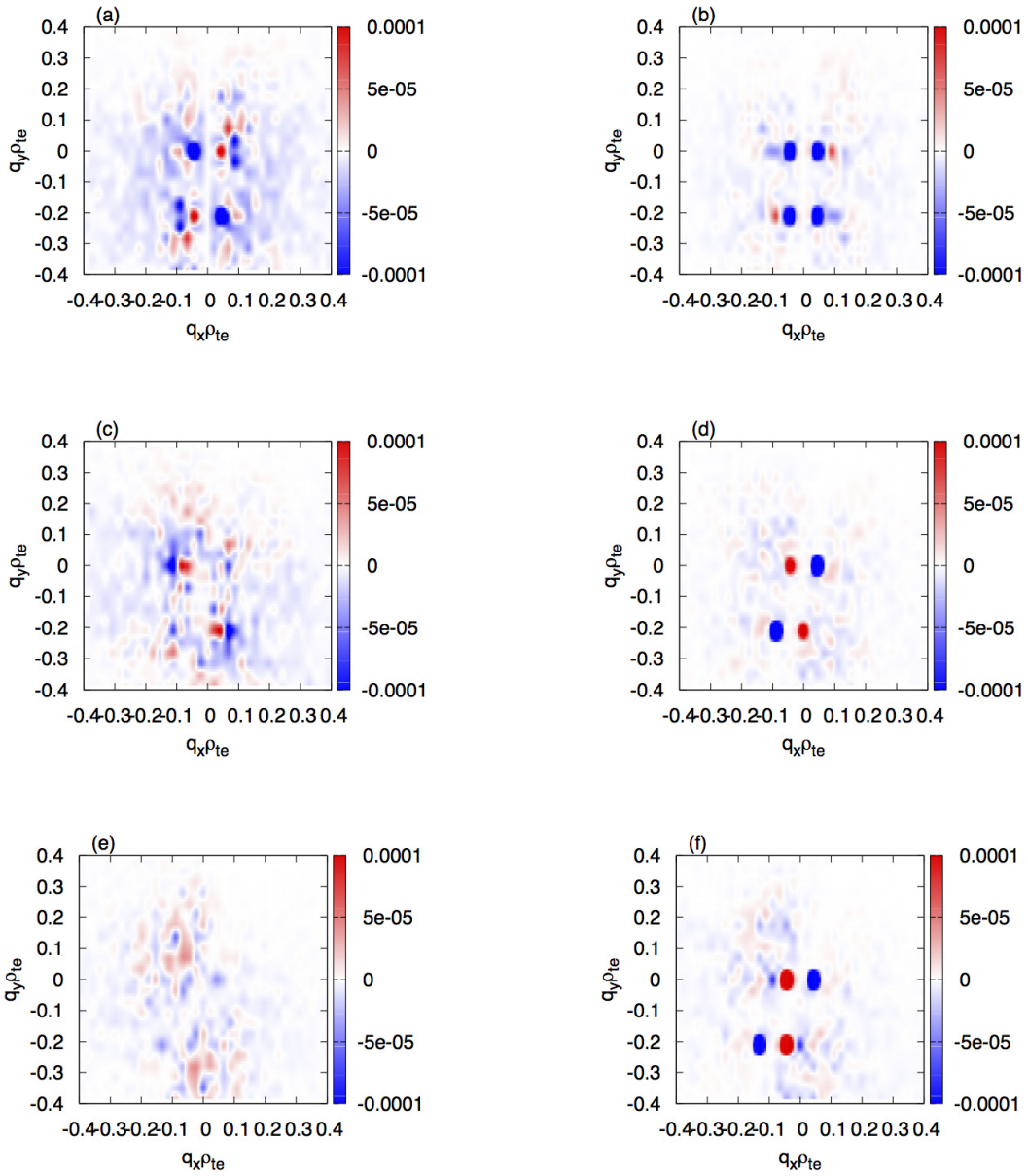

Fig. 5 Wavenumber spectra of the entropy transfer function normalized to the sum of the transport terms, $\overline{\mathcal{J}}_e[\mathbf{p}_\perp|\mathbf{q}_\perp,\mathbf{k}_\perp]/\overline{\mathcal{F}}_e$ for $(p_x\rho_{te},\ p_y\rho_{te}) = (0,\ 0.21)$, $(0.044,\ 0.21)$ and $(0.088,\ 0.21)$ with the fixed $p_y\rho_{te} = 0.21$ in the steady state for the adiabatic (left column) and kinetic ion (right column) cases, where the time-average is taken over $2300\,(L_n/v_{te}) \le t \le 2500\,(L_n/v_{te})$. The successive entropy transfer of the dominant ETG mode into the high radial wavenumber region is found in the ETG-TEM turbulence ((b), (d) and (f)), but not in the ETG turbulence ((a), (c) and (e)).

with $(p_x\rho_{te},\ p_y\rho_{te}) = (0, 0.21)$ dominantly interacts with the other non-zonal mode $(q_x\rho_{te},\ q_y\rho_{te}) = (-0.044, -0.21)$ via the zonal mode $(k_x\rho_{te},\ k_y\rho_{te}) = (0.044, 0)$. It is also found in Fig. 5 (d) that the $(p_x\rho_{te},\ p_y\rho_{te}) = (0.044, 0.21)$ mode interacts with $(q_x\rho_{te},\ q_y\rho_{te}) = (-0.088, -0.21)$ via the zonal mode with $(k_x\rho_{te},\ k_y\rho_{te}) = (0.044, 0)$. Considering the reality condition of the physical variables, it is shown that the $-\mathbf{q}_\perp$ mode is equivalent to the $\mathbf{q}_\perp$ mode. Thus, it can be rephrased that the $(p_x\rho_{te},\ p_y\rho_{te}) = (0.044, 0.21)$ mode transfers the entropy to the $(q_x\rho_{te},\ q_y\rho_{te}) = (0.088, 0.21)$ via the zonal mode. In the same way, the $(p_x\rho_{te},\ p_y\rho_{te}) = (0.088, 0.21)$ mode transfers the entropy to the $(q_x\rho_{te},\ q_y\rho_{te}) = (0.132, 0.21)$ via the zonal mode as shown in Fig. 5 (f). These figures show that the TEM-driven zonal flow contributes to the successive entropy transfer of the ETG mode in the radial wavenumber direction. In the adiabatic ion case, however, there is no clear spectral structure suggesting the successive entropy transfer to the non-zonal modes with higher radial wavenumbers (See Figs. 5 (a), (c) and (e)) which is consistent with the earlier work [11]. It is concluded that the successive entropy transfer to the higher wavenumber mode in the adiabatic ion case is much weaker than in the kinetic ion case.

The successive entropy transfer process in the kinetic ion case is summarized in Fig. 6. Figure 6 (a) shows

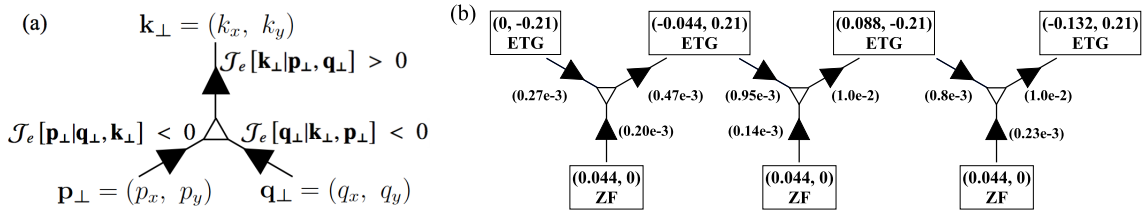

Fig. 6 Diagram for the nonlinear entropy transfer in the perpendicular wavenumber space: (a) an element of the diagram which represents the relationships between the three different modes $\mathbf{k}_\perp$, $\mathbf{p}_\perp$ and $\mathbf{q}_\perp$, (b) the diagram of the entropy transfer of the ETG modes under the TEM-driven zonal flow. The successive entropy transfer from the ETG mode with low k_x to high k_x is shown.

the element of the diagram which represents the relationships among the three different modes $\mathbf{k}_\perp$, $\mathbf{p}_\perp$ and $\mathbf{q}_\perp$ (see Ref. [13] for details). The arrows represent signs of $\overline{\mathcal{J}}_{\rm e}[\mathbf{k}_\perp|\mathbf{p}_\perp,\mathbf{q}_\perp]$, $\overline{\mathcal{J}}_{\rm e}[\mathbf{p}_\perp|\mathbf{q}_\perp,\mathbf{k}_\perp]$ and $\overline{\mathcal{J}}_{\rm e}[\mathbf{q}_\perp|\mathbf{k}_\perp,\mathbf{p}_\perp]$, respectively, where $\overline{\mathcal{J}}_{\rm e}[\mathbf{k}_\perp|\mathbf{p}_\perp,\mathbf{q}_\perp] > 0$, $\overline{\mathcal{J}}_{\rm e}[\mathbf{p}_\perp|\mathbf{q}_\perp,\mathbf{k}_\perp] < 0$ and $\overline{\mathcal{J}}_{\rm e}[\mathbf{q}_\perp|\mathbf{k}_\perp,\mathbf{p}_\perp] < 0$ in Fig. 6 (a). Figure 6 (b) shows the diagram for the entropy transfer process in the steady state of ETG-TEM turbulence. As shown in Fig. 5 (b), the contour plot of $\overline{\mathcal{J}}_{\rm e}[\mathbf{p}_\perp|\mathbf{q}_\perp,\mathbf{k}_\perp]/\overline{\mathcal{F}}_{\rm e}$ has the peaks with negative values at $(q_x\rho_{\rm te},\ q_y\rho_{\rm te}) = (-0.044, -0.21)$ and $(k_x\rho_{\rm te},\ k_y\rho_{\rm te}) = (0.044,\ 0)$, representing the entropy transfer from $(p_x\rho_{\rm te},\ p_y\rho_{\rm te}) = (0,\ 0.21)$ to $(q_x\rho_{\rm te},\ q_y\rho_{\rm te}) = (-0.044, -0.21)$ and zonal mode $(k_x\rho_{\rm te},\ k_y\rho_{\rm te}) = (0.044,\ 0)$. This triad interaction is summarized in Fig. 6 (b), where the ETG mode $(p_x\rho_{\rm te},\ p_y\rho_{\rm te}) = (0.044,\ 0.21)$ receives the entropy from the ETG mode $(p_x\rho_{\rm te},\ p_y\rho_{\rm te}) = (0,\ 0.21)$ with the value of 0.26×10^{-3} and from the zonal mode $(k_x\rho_{\rm te},\ k_y\rho_{\rm te}) = (0.044,\ 0)$ with the value of 0.2×10^{-3}. In total, the ETG mode $(p_x\rho_{\rm te},\ p_y\rho_{\rm te}) = (0.044,\ 0.21)$ receives the entropy of 0.46×10^{-3}.

Figure 5 (d) shows that the $\overline{\mathcal{J}}_{\rm e}[\mathbf{p}_\perp|\mathbf{q}_\perp,\mathbf{k}_\perp]/\overline{\mathcal{F}}_{\rm e}$ has the peaks with negative values at $(q_x\rho_{\rm te},\ q_y\rho_{\rm te}) = (-0.088, -0.21)$ and $(k_x\rho_{\rm te},\ k_y\rho_{\rm te}) = (0.044,\ 0)$, representing the entropy transfer from $(p_x\rho_{\rm te},\ p_y\rho_{\rm te}) = (0.044,\ 0.21)$ to $(q_x\rho_{\rm te},\ q_y\rho_{\rm te}) = (-0.088, -0.21)$ and the zonal mode $(k_x\rho_{\rm te},\ k_y\rho_{\rm te}) = (0.044, 0)$. The positive peaks at $(q_x\rho_{\rm te},\ q_y\rho_{\rm te}) = (0, -0.21)$ and $(k_x\rho_{\rm te},\ k_y\rho_{\rm te}) = (-0.044,\ 0)$ mean that the $(p_x\rho_{\rm te},\ p_y\rho_{\rm te}) = (0.044,\ 0.21)$ mode receives the entropy from the primary mode $(p_x\rho_{\rm te},\ p_y\rho_{\rm te}) = (0,\ 0.21)$ and the zonal mode $(k_x\rho_{\rm te},\ k_y\rho_{\rm te}) = (-0.044,\ 0)$. In summary, the ETG mode with $(p_x\rho_{\rm te},\ p_y\rho_{\rm te}) = (0.044,\ 0.21)$ receives the entropy from the $(p_x\rho_{\rm te},\ p_y\rho_{\rm te}) = (0,\ 0.21)$ mode and then sends the entropy to the $(p_x\rho_{\rm te},\ p_y\rho_{\rm te}) = (0.088,\ 0.21)$, which means the successive entropy transfer from the dominant ETG mode to the high radial wavenumber region via TEM driven zonal flow. Similarly, Fig. 4 (f) shows that the $(p_x\rho_{\rm te},\ p_y\rho_{\rm te}) = (0.088, 0.21)$ mode receives the entropy from the $(p_x\rho_{\rm te},\ p_y\rho_{\rm te}) = (0.044, 0.21)$ and then transfers to the $(q_x\rho_{\rm te},\ q_y\rho_{\rm te}) = (0.132, 0.21)$ (see the rightmost element of the diagram in Fig. 6 (b)). Again, this is a part of successive entropy transfer process of ETG modes by the TEM driven zonal flow.

4.3 Difference in fluctuation spectra

In this subsection, we present the impact of the successive entropy transfer on the wavenumber spectra of fluctuations. Figures 7 (a) and (b) show the normalized power spectra of potential fluctuation $\overline{\langle|\delta\phi_{k_\perp}|^2\rangle}\ /\ \sum_{k_y\neq0}\overline{\langle|\delta\phi_{k_\perp}|^2\rangle}$ for the adiabatic and kinetic ion cases, where time-average is taken over $2300\,(L_n/v_{\rm te}) \le t \le 2500\,(L_n/v_{\rm te})$. It is found that the wavenumber spectra of electrostatic potential in the kinetic ion case is more expanded in the high k_x region (shown in Fig. 7 (b)) than in the adiabatic ion case (shown in Fig. 7 (a)).

Figures 7 (c) and (d) show the normalized spectra of the energy flux $\overline{Q}_{{\rm e}k_\perp}\ /\ \sum_{k_\perp}\overline{Q}_{{\rm e}k_\perp}$ (defined in Eq. (9)) for the adiabatic and kinetic ion cases.

The spectrum of the energy flux in the kinetic ion case is also found broadened in the radial wavenumber direction compared to the adiabatic ion case. The broader wavenumber spectrum in the kinetic ion case is considered as a consequence of the successive entropy transfer process in the ETG modes via the TEM-driven zonal flow. The similar broadening of the fluctuation spectrum has been also reported in the toroidal ITG turbulence, and is attributed to the successive entropy transfer via ITG-driven zonal flows [11]. Here, it should be emphasized that the TEM-driven zonal flows effectively regulate the different kind of turbulence with high wave numbers, that is, the ETG turbulence, leading to modification of the turbulent fluctuation spectra. This is not the case for the ITG turbulence, where the ITG turbulence is regulated by the self-generated zonal flows.

5. Summary

In this work, the entropy transfer analysis [11] was applied to the previous gyrokinetic simulation data of pure ETG and ETG-TEM turbulence in order to examine the regulation process of ETG modes found in the ETG-TEM turbulence simulation [10]. In Ref. [10], we showed that the transport level in the ETG-TEM turbulence is much lower than in the pure ETG turbulence. It turned out that the lower transport level in the ETG-TEM turbulence stems from the stronger zonal flows driven by TEMs. In order to understand the role of zonal flow, the entropy transfer process was investigated for the saturation and steady-state phases of pure ETG and ETG-TEM turbulence. Relation-

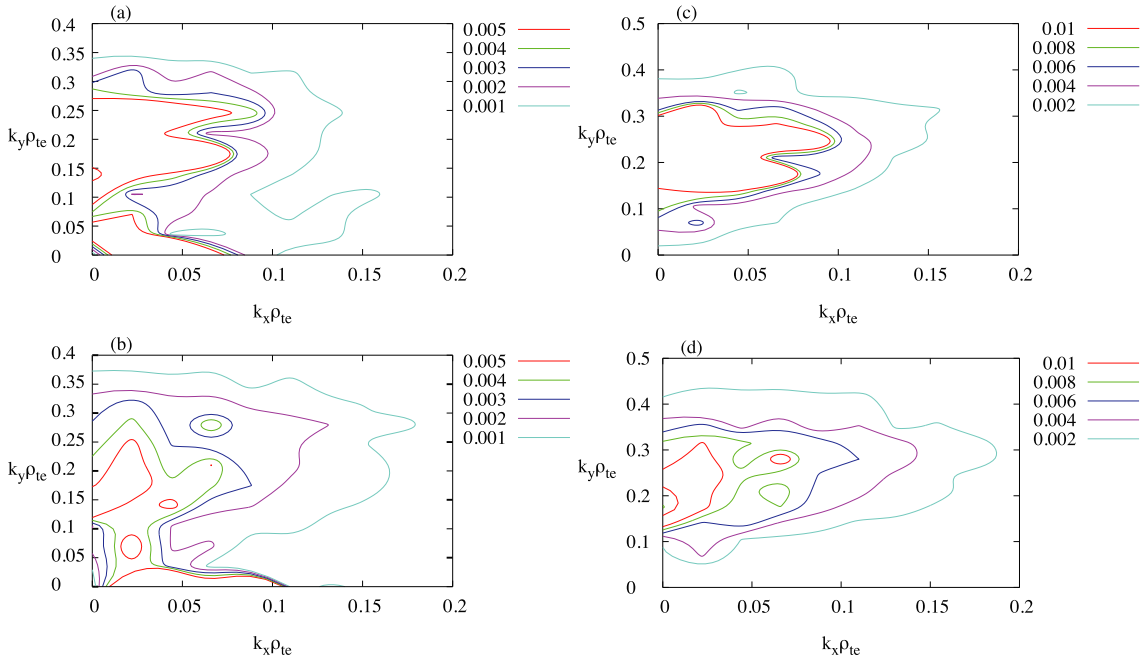

Fig. 7 Wavenumber spectra of the normalized potential fluctuation $\overline{\langle|\delta\phi_{k_\perp}|^2\rangle}$ / $\sum_{k_y\neq 0}\overline{\langle|\delta\phi_{k_\perp}|^2\rangle}$ [(a) and (b)] and the normalized energy flux $\overline{Q}_{ek_\perp}$ / $\sum_{k_\perp}\overline{Q}_{ek_\perp}$ [(c) and (d)] in the steady states of the adiabatic ion (upper row) and kinetic ion (lower row) cases, where time-average is taken over $2300\,(L_n/v_{te}) \le t \le 2500\,(L_n/v_{te})$. The wavenumber spectra for the ETG-TEM turbulence ((b) and (d)) are broadened in the radial wavenumber direction, while those for the ETG turbulence ((a) and (c)) are confined in the lower radial wavenumber region.

ships between the entropy transfer and the wavenumber spectra of electrostatic potential fluctuations and energy flux were also discussed.

First, we have confirmed conservation of the quadratic quantities, i.e. the entropy balance relation [11, 16], which provides a solid basis for the entropy transfer analysis. Then, the source of zonal flows for both simulations were investigated by means of the entropy transfer analysis. We identified the entropy transfer from the low wavenumber TEMs to zonal flows in the ETG-TEM turbulence, whereas the entropy transfer from the high wavenumber ETG modes to zonal flows was found in the ETG turbulence. It is concluded that the strong zonal flow found in the ETG-TEM turbulence is driven by TEMs. The difference in the zonal flow amplitudes is explained by the larger residual zonal flow level at low wavenumber TEM scale than at high wavenumber ETG scale as discussed in Ref. [10].

The role of the zonal flows in steady state was also investigated. In the ETG-TEM turbulence, it turned out that the zonal flows meditate the entropy transfer of the ETG modes from low to high radial wavenumber regions. The successive entropy transfer broadens the fluctuation spectrum in the radial wavenumber direction. The high radial wavenumber modes are stabilized by the finite Larmor radius effect and less likely contribute to energy transport. Thus the successive entropy transfer results in the transport reduction. These characteristics of TEM driven zonal flows in the ETG-TEM turbulence are quite similar to those of ITG driven zonal flows in the ITG turbulence [11]. In contrast, in the situation where ETG modes are unstable but TEMs are stable, the pure ETG turbulence does not produce strong zonal flows, leading to a relatively narrow spectrum in the radial wavenumber direction. Through nonlinear entropy transfer analysis, it was shown that instabilities with the different scales, such as ETG modes and TEMs can interact via zonal flows.

Acknowledgments

This work is supported in part by the NIFS collaborative Research Programs, NIFS14KNTT026. The numerical simulations were performed as a part of GTNAXIS project on the Helios Super Computer System at the Computational Simulation Center of the International Fusion Energy Research Center (IFERC). The authors thank Dr. M. Nakata and Dr. S. Maeyama for helpful discussions about entropy transfer analysis.

[1] W. Horton, Rev. Mod. Phys. **71**, 735 (1999).
[2] W.M. Tang, Nucl. Fusion **18**, 1089 (1978).
[3] W. Dorland, F. Jenko, M. Kotschenreuther and B.N. Rogers, Phys. Rev. Lett. **85**, 5579 (2000).
[4] F. Jenko, W. Dorland, M. Kotschenreuther and B.N. Rogers, Phys. Plasmas **7**, 1904 (2000).
[5] X. Garbet, Y. Idomura, L. Villard and T.-H. Watanabe, Nucl. Fusion **50**, 043002 (2010).
[6] T.L. Rhodes, C. Holland, S.P. Smith, A.E. White, K.H. Burrell, J. Candy, J.C. DeBoo, E.J. Doyle, J.C. Hillesheim,

J.E. Kinsey, G.R. McKee, D. Mikkelsen, W.A. Peebles, C.C. Petty, R. Prater, S. Parker, Y. Chen, L. Schmitz, G.M. Staebler, R.E. Waltz, G. Wang, Z. Yan and L. Zeng, Nucl. Fusion **51**, 063022 (2011).

[7] M. Nunami, T.-H. Watanabe, H. Sugama and K. Tanaka, Phys. Plasmas **19**, 042504 (2012).

[8] P.H. Diamond, S.-I. Itoh, K. Itoh and T.S. Hahm, Plasma Phys. Control. Fusion **47**, R35 (2005).

[9] B.W. Stallard, C.M. Greenfield, G.M. Staebler, C.L. Rettig, M.S. Chu, M.E. Austin, D.R. Baker, L.R. Bayor, K.H. Burrell, J.C. DeBoo, J.S. DeGrassie, E.J. Doyle, J. Lohr, G.R. McKee, R.L. Miller, W.A. Peebles, C.C. Petty, R.I. Pinsker, B.W. Rice, T.L. Rhodes, R.E. Waltz, L. Zeng and the DIII-D Team, Phys. Plasmas **6**, 1978 (1999).

[10] Y. Asahi, A. Ishizawa, T.-H. Watanabe, H. Tsutsui and S. Tsuji-Iio, Phys. Plasmas **21**, 052306 (2014).

[11] M. Nakata, T.-H. Watanabe and H. Sugama, Phys. Plasmas **19**, 022303 (2012).

[12] T.-H. Watanabe, H. Sugama, M. Nunami, K. Tanaka and M. Nakata, Plasma Phys. Control. Fusion **55**, 014017 (2013).

[13] A. Ishizawa, T.-H. Watanabe, H. Sugama, S. Maeyama and N. Nakajima, Phys. Plasmas **21**, 055905 (2014).

[14] A. Ishizawa, S. Maeyama, T.-H. Watanabe and H. Sugama, Nucl. Fusion **53**, 053007 (2013).

[15] T.-H. Watanabe and H. Sugama, Nucl. Fusion **46**, 24 (2006).

[16] H. Sugama, T.-H. Watanabe and M. Nunami, Phys. Plasmas **16**, 112503 (2009).

[17] Y. Xiao and P.J. Catto, Phys. Plasmas **13**, 102311 (2006).

[18] L. Wang and T.S. Hahm, Phys. Plasma **16**, 062309 (2009).

[19] F. Jenko and A. Kendl, Phys. Plasmas **9**, 4103 (2002).